LARGE-SCALE LNG AND LPG POOL FIRES

G.A. Mizner and J.A. Eyre*

Tests have been carried out to measure the thermal radiation from 20 m diameter land-based pool fires of LNG, LPG and kerosine. Both wide- and narrow-angle radiometers were used to measure thermal radiation; other measurements included the mass burning rate and composition of the fuel, and metal surface temperatures close to the fire. The average surface emissive power of the LNG fire was determined to be 153 kW/m^2; the narrow-angle radimeters gave maximum values greater than 200 kW/m^2. Copious quantities of soot, formed during the LPG and kerosine fires, led to average surface emissive powers of 48 kW/m^2 and approximately 35 kW/m^2 respectively.

INTRODUCTION

Calculation of the thermal radiation from large liquefied gas fires is a necessary part of an overall hazard assessment of storage facilities. For such calculations knowledge of the radiant power of the flame is required, together with its size and shape, and an assessment of the atmospheric transmission losses between the flame and the target.

Theoretical prediction of the radiant power is not at present practicable because a number of the parameters associated with large turbulent diffusion flames, such as the soot concentration and the temperature variation of the gases throughout the flame, cannot be accurately determined for a given fire. There is, therefore, a need for these large fires to be characterised experimentally.

Many LNG pool fire tests have been carried out but, for practical reasons, most of them have been with small diameter pools where the surface flux of the flames was not close to the limiting value. Several of these tests were in any case part of a programme for testing fire suppresion systems so that radiation measurements were of secondary importance. A detailed survey of the more important of these tests has been made by the American Gas Association (1). The most extensive series of tests to determine the radiative properties of LNG pool fires were those sponsored by the American Gas Association (1). The series included 1.8 m and 6 m diameter LNG fires, as well as one 24 m fire which unfortunately yielded no useful radiation data because of instrument failure. As a consequence, the limiting value of the surface flux for large fires remained undetermined. There is, therefore, a need for more data from large fires, and this is particularly so

* Shell Research Ltd., Thornton Research Centre, P.O. Box 1, Chester CH1 3SH

for LPG for which few previous data exist. Consequently, the 20 m pool fire tests described in this paper were conducted. The programme included one LNG and one LPG test, as well as a kerosine fire which tested the instrumentation and provided comparable data for a typical liquid fuel.

TEST FACILITY AND MEASUREMENTS

The fires were conducted in a 20 m circular bund located in one corner of an existing 100 m square concrete pad, Figure 1. The height of the bund walls was 300 mm, and the whole structure was covered with a protective layer of insulating concrete. The bund was pre-cooled with liquid nitrogen prior to admitting the LNG or LPG. The fuel was supplied simultaneously from three road tankers, located about 60 m from the bund, via three insulated stainless steel pipes.

Twenty-one wide-angle radiometers were used to measure the radiation flux at locations which were well spread around the fire. The layout during the LNG fire is shown in Figure 1. The radiometers were Land type rad/P which have a response time of approximately 1 s to reach 90% of a step signal and 2 s to reach 98%, and have an angle of complete vision of 50°. All the radiometers were fitted with 2 mm thick calcium fluoride windows, and were calibrated by the manufacturers in front of a black-body source at 1000°C with the windows in place. Check calibrations were also made in the laboratory both before and after the tests, and in all cases agreed with the quoted calibrations to within 3%.

In addition to the wide-angle instruments, two narrow-angle radiometers were deployed, Figure 1. They were constructed by reducing the viewing angle of two Land rad/P wide-angle radiometers to 6.4°. The advantage of narrow-angle instruments is that provided their field of view is completely filled with flame, then they measure directly the surface flux, apart from a correction for the atmospheric transmission losses.

Six metal plate assemblies were constructed to measure metal surface temperatures, and also to permit measurement of radiation fluxes closer to the fire than could be achieved with the radiometers. The steel plates were 0.17 m × 0.17 m × 0.003 m and were insulated on the rear face with a 25 mm layer of Sindanyo. A chromel/alumel thermocouple was welded to the centre of the rear face and the outer surface was painted with a high solids EPIKOTE paint. The plates were located 1.5 and 2 diameters from the bund centre as shown in Figure 1.

During the LNG and LPG fires samples were taken at regular intervals from both the liquid pool and the vapour just above the liquid surface. The samples were drawn through 3 mm i.d. tubes by an evacuated vessel and were diverted into small sample bottles as required. The time to fill one bottle was about 45 s, so that the samples represented an average over that period. Liquid samples were taken every two minutes and gas samples every minute during the fire.

The liquid level in the bund was monitored using a 'bubbler' gauge. Gaseous nitrogen was passed through a tube whose open end was located on the floor of the bund. The pressure required to maintain a steady flow of nitrogen was related to the depth of liquid in the bund. The system was calibrated using a variety of liquids including LNG, LPG, kerosine and water.

The primary ignition system for the liquefied gas tests was a propane torch which was lit at the upwind edge of the bund by a high-tension spark. Fast burning igniter cord was used as a back-up system.

Other measurements included the wind speed and direction and the relative humidity. Photographic records were obtained from two locations which were approximately upwind and crosswind to the fire. At each location colour video and still photography were employed.

RESULTS

Gas and Liquid Compositions

The gas and liquid compositions during the LNG fire are shown in Figure 2. Initially the methane content of the combustible gas was at least 90%. Although this gradually declined during the burn, it remained above 70% until the sixth minute. The proportion of methane in the liquid pool decreased steadily in favour of ethane, as would be expected from their respective boiling points.

During the LPG fire the composition stabilised at about 60% propane and 40% propene.

Flame Shape and Appearance

An outline of the LNG flame viewed from almost crosswind one minute after ignition is shown in Figure 3. The shaded areas represent the regions of black soot. Even at this early stage of the fire the flame was sooty in its upper regions. Although this may have been enhanced by the 10% ethane content at that stage, the appearance of black soot was due to oxygen starvation which is characteristic of such large fires. Certainly, the flame became sootier as the fire progressed, with a significant increase after the fifth minute when the ethane content increased rapidly as shown in Figure 2.

The flame appeared to be roughly cylindrical in shape. As can be seen from Figure 3 the base of the flame extended well beyond the bund wall in the downwind direction. The size of this "spill-over" was between 5 m and 10 m which is a significant proportion of the bund diameter and clearly should be accounted for when modelling the flame shape. For the view factor calculations, which will be described later, the flame shape was represented by a tilted cylinder. The horizontal base of a tilted cylinder is elliptical with the major or downwind axis, which depends on the tilt angle, longer than the crosswind axis, which was set equal to the pool diameter. In order to obtain the best fit to the flames in the downwind sector, where the bulk of the radiation measurements were made, the base of the model cyclinder was moved so that the downwind edge of the ellipse coincided with the observed edge of the flame 'spill-over'. This resulted in a downwind movement of the flame centre of upto 2.5 m. The upwind flame edge, which was actually coincident with the edge of the bund, was, however, not so accurately represented.

Figure 4 shows the outline of the LPG flame 70 s after ignition. Once again the shaded areas represent the regions of black soot. It is noticeable that there was considerably more soot than during the LNG fire, and that the soot enveloped a substantial portion of the luminous flame. The appearance of the fire did not change during the burn which is consistent with the stable composition. As in the LNG case the flame shape, as indicated by the

extremities of the luminous flame, can be represented by a tilted cylinder. The downwind flame "spill-over" was again evident and varied in this case between 5 m and 11 m beyond the bund wall.

During the kerosine fire the soot was so dense that the flame dimensions were extremely difficult to determine. However, it might be expected that the flame shape would have been similar to that observed during the LNG and LPG tests.

Burning Rate

The burning rates measured using the 'bubbler' gauge were 0.106 kg/m^2 s (2.37×10^{-4} m/s) for LNG and 0.13 kg/m^2 s (2.17×10^{-4} m/s) for LPG. During both fires the liquid regression rates remained remarkably constant until close to the end. The LNG value compares well with that of 2.54×10^{-4} m/s estimated for large fires by Welker from the AGA tests (1). The LPG value is slightly higher than that for LNG and this is consistent with its lower heat of vaporisation per kilogram at its boiling point. For kerosine the burning rate was found to be 0.06 kg/m^2 s (0.76×10^{-4} m/s) which is consistent with a value of 0.67×10^{-4} m/s obtained by Hägglund and Persson (2) for fires up to 10 m in diameter.

Flame Length

The mean luminous flame lengths measured from the video recordings are shown in Figure 5 for both the LNG and LPG fires. For LNG the average during the first 4 minutes of the fire was 43 m (L/D = 2.15). Thereafter, it fell as the increasing quantity of soot masked the upper regions of the flame. Generally, the standard deviation about the mean flame lengths was about 10%. For LPG the average value was 47 m (L/D = 2.35) which is longer than that for LNG and is consistent with the higher mass burning rate. The standard deviation was about 18%, and this larger fluctuation than during the LNG fire was noticeable on the video recordings, where it could be seen quite clearly that with a periodicity of about 4 s the fire built up to a length of greater than 60 m and then the top portion burnt out to leave a flame only 30 m long.

During the kerosine fire the luminous flame length, as far as it was visible, was generally between 30 and 38 m.

The correlation most commonly used for the prediction of flame length as a function of pool size and mass burning rate is that derived by Thomas (3) from experiments with wood cribs in still air:

$$L/D = 42 \left(\frac{\dot{m}}{\rho_a \sqrt{gD}}\right)^{0.61} \qquad \ldots\ldots (1)$$

If the measured burning rates are used in equation (1), the values of L/D are 1.88 and 2.13 for LNG and LPG respectively. These values underestimate the observed mean flame lengths by 12.6% for LNG and 9.4% for LPG. For kerosine, equation 1 gives a flame length of 1.33D whereas the observed flame length appeared to be between 1.5D and 1.9D.

Tilt Angle

Based on the AGA tests (1), Atallah and Raj derived the following correlation for the flame tilt angle:

$$\cos\theta = 1, \quad U^* < 1$$

$$\cos\theta = \frac{1}{\sqrt{U^*}}, \quad U^* > 1 \qquad \ldots\ldots (2)$$

where $U^* = \dfrac{U_w}{\left(\dfrac{\dot{m}}{\rho_v} gD\right)^{1/3}}$, and U_w is the wind speed.

Another correlation was derived by Welker and Sliepcevich (4) and shown to fit the AGA data (1):

$$\frac{\tan\theta}{\cos\theta} = 3.2 \left(\frac{U_w D}{\nu_a}\right)^{0.07} \left(\frac{U_w^2}{gD}\right)^{0.7} \left(\frac{\rho_v}{\rho_a}\right)^{-0.6} \qquad \ldots\ldots (3)$$

The angles predicted by both the above correlations are compared in Table 1 with those observed during the LNG and LPG fires. The agreement is good for both correlations. Although only two experimental points have been used for comparison, and at similar wind speeds, they have both also shown good agreement with previous data.

TABLE 1 - Comparison of Predicted and Observed Tilt Angles

Test	Windspeed (m/s)	Observed Tilt Angle (deg.)	Predicted Tilt Angles (deg.)	
			Atallah and Raj (AGA (1))	Welker and Sliepcevich (4)
LNG	6.15	54.0	52.5	54.9
LPG	6.6	53.0	54.4	53.9

Radiation Flux

Three radiometer outputs, one from each of the three fires, are shown in Figure 6; all the radiometer outputs were averaged over 30 s periods. The radiation intensities are directly comparable because the radiometers were at similar locations relative to the fires. The effect of the large quantities of soot during the LPG and kerosine fires is evident. The measured radiation flux during the LNG fire was approximately 2.5 to 3 times greater than that during the LPG fire, and 5 times greater than that during the kerosine fire. The radiation fluxes measured around the LNG fire correlated well with the location of the measuring station relative to the wind direction; the maximum fluxes at a particular distance from the bund were recorded downwind, and variations in the wind direction could be detected from the radiometer outputs. During the LPG and kerosine fires the tendency for the soot concentration to be higher in the downwind portions of the flame meant that the measured radiation fluxes depended in addition on the proportion of flame or soot that the radiometer viewed.

Solid Flame Model

In order to determine the surface emissive powers of the flames a solid flame model has been adopted which assumes that the flame may be represented by a solid body radiating from its surface, area A_1, with an average surface emissive power, E. Then, the thermal radiation q received by an element A_2 is given by:

$$q = F_{1-2} E A_1 \tau \qquad \ldots\ldots (4)$$

where F_{1-2}, the view factor, is a measure of how much of the field of view of A_1 is occupied by A_2, and τ is the atmospheric transmission coefficient. The reciprocal theorem for view factors gives

$$A_1 F_{1-2} = A_2 F_{2-1}$$

Therefore from equation 4 the heat received per unit area at A_2 is:

$$\frac{q}{A_2} = F_{2-1} E \tau \qquad \ldots\ldots (5)$$

and $\frac{q}{A_2}$ is the quantity measured by the radiometer.

View Factor

The view factor for an infinitesimal surface element δA_2 can be expressed as

$$F_{2-1} = \sum_{A_1} \frac{\cos \phi_1 \cos \phi_2 \, \delta A_1}{\pi R^2} \qquad \ldots\ldots (6)$$

where ϕ_1 and ϕ_2 are the angles between the normals to the elements δA_1 and δA_2 and the line joining the elements, length R. The summation in equation 6 was performed by splitting the adopted flame shape into 10^4 surface elements. The flame geometry chosen was a tilted cylinder which was previously shown to be representative of the observed flame shape; measured values of the flame length and tilt angle were used in the calculations.

Transmission Coefficient

Absorption of infra-red radiation by the atmosphere between the flame and the receiver is significant when distances of greater than a few metres are involved. Water vapour and carbon dioxide are the principal atmospheric constituents which absorb in the infra-red. Correction of the measured radiation fluxes for these transmission losses requires a detailed knowledge of the spectrum of the radiation emitted from the flame, and the monochromatic atmospheric transmissivities as a function of distance and humidity. Unfortunately, reliable emission spectra from large fires, especially in the strong CO_2 and H_2O bands, are still not available. Therfore, all the radiation fluxes measured during these fires have been corrected using the data derived by Raj (5) assuming the emitting source to be a black body at 1150 K. Whilst it is recognised that the use of these data from a black body is not entirely correct, and that the temperature of 1150 K may not be the

best one to use, a more accurate analysis must await more complete spectral data. In the meantime, the same set of data should be used for radiation flux predictions to ensure consistency between the measured and predicted values. As an example, the use of these data for the LNG fire, during which the ambient temperature was 27°C and the relative humidity 53%, produced values of the transmission coefficient ranging from 0.75 at 30 m to 0.67 at 110 m.

Surface Emissive Powers

Using the view factor and transmission coefficients described above, the average surface emissive powers were calculated using equation (5). The values for the LNG fire are shown in Figure 7 at 30 s intervals. The surface emissive power was calculated independently for each radiometer and the value shown is the mean. The accompanying error bars represent the standard deviations around the mean value. In general, the standard deviation was around 10% or less. This is a good indication of the accuracy with which the flame shape can be represented by a tilted cylinder because the radiometers were deployed around the bund and had differing views of the fire. Figure 7 indicates that the mean surface emissive power was fairly steady until 5 minutes into the burn, after which it fell as the soot concentration increased. The average value over the steady period was 153 kW/m^2.

The surface emissive powers calculated for the LPG fire are shown in Figure 8. The mean power remained steady until the fire began to die out. The average value up to 4.5 minutes is 48 kW/m^2. It is noticeable that the standard deviations are larger than during the LNG fire, typically between 15% and 25%. This is because of the high soot concentration which caused the proportion of unobstructed flame viewed to vary amongst the radiometers.

The wide-angle radiation fluxes from the kerosine fire have not been converted to average surface emissive powers because of the difficulties in determining the dimensions of the sooty flame.

Narrow-Angle Radiometers

The two narrow-angle radiometers were aimed 6.8 m and 12.2 m above the centre of the bund. When these instruments had their field of view completely filled by the flame their outputs, after correction for atmospheric transmission losses, gave a direct measurement of the surface emissive power. The values for all three fires are presented in Table 2. During the LNG fire the field of view of radiometer N3 was completely filled with flame until the fire began to die out beyond the fifth minute. Radiometer N4, which was aimed higher up, also saw only flame during the main burning period except between 1 and 2 minutes after ignition, thereby explaining the lower readings at that time. Between 2.5 and 4.5 minutes the readings from N3 and N4 were very similar, suggesting that the values during this period are those most representative of this LNG flame. The maximum value during this period was 219 kW/m^2 from radiometer N4 three minutes into the fire.

During the LPG fire, radiometer N3 viewed only flame, but N4 did not have its field of view completely filled, hence the lower readings from N4. The mean value from N3 is about 49 kW/m^2, which is close to that from the wide-angle radiometers. It might be expected that the narrow-angle radiometer should give a higher value because of its restricted view. However, in this case, inspection of photographs revealed that N3 viewed a substantial proportion of soot as well as flame. Had it been aimed even lower down the flame it may well have measured higher values.

TABLE 2 - Surface Emissive Powers Measured by the Narrow-Angle Radiometers

Time (min)	Surface Emissive Power, E (kW/m²)					
	LNG		LPG		Kerosine	
	N3	N4	N3	N4	N3	N4
0.5	176.05	171.59	47.52	23.94	24.38	32.61
1.0	148.54	120.42	48.24	24.30	36.02	34.49
1.5	170.18	156.11	48.96	24.66	35.33	30.88
2.0	170.54	156.97	50.03	25.73	37.17	29.27
2.5	195.48	205.13	50.03	26.08	38.75	32.88
3.0	203.92	219.75	50.38	23.94	37.38	30.88
3.5	199.51	213.30	48.96	22.40	33.76	25.67
4.0	177.87	175.88	48.96	21.44	37.17	29.27
4.5	184.48	182.34	50.03	23.94	-	-
5.0	161.38	154.38	41.10	13.22	36.94	29.27
5.5	137.90	120.42	23.94	8.58	-	-

Radiometer N3 aimed 6.8 m above bund floor

Radiometer N4 aimed 12.2 m above bund floor

For the kerosine fire, N3 once again had its field of view completely filled with flame/soot, but for N4 the situation was less certain. The values from N3 are a clear indication of the effectiveness of the soot in reducing the radiation incident upon a target. Although the radiation fluxes from the wide-angle radiometers were not converted to surface emissive powers, it is clear from their magnitude and the narrow-angle values that the effective power of the kerosine fire is only about one fifth of that of the LNG flame.

Metal Plate Temperatures

Surface temperatures were measured on six metal plates at distances closer to the fires than was possible with the radiometers. The temperature-time profiles from one of the plates during each fire are shown in Figure 9; in each case the plate concerned was almost downwind and was 30 m (1.5 D) from the centre of the bund. The profile recorded during the LNG fire shows that the temperature peaked at 480°C approximately 5 minutes after ignition. The plateau was due to a slight change in the wind direction, and the subsequent fall in temperature beyond the fifth minute occurred as the fire became sootier towards the end of the test. For a fire of longer duration an equilibrium temperature higher than the maximum recorded here would have been

reached. The profiles from the LPG and kerosine fires indicate, as expected, that the heating rate was considerably lower than from the LNG fire. The LPG profile indicates that the temperature was still rising towards the end of the test, but for the kerosine fire, which lasted for more than 8 minutes, an equilibrium value appears to have been reached.

An estimate of the radiation flux incident on the plates can be made using the temperature profiles, such as those in Figure 9, and the heat balance equation:

$$\rho c d \frac{dT_s}{dt} = \alpha q(t) - \sigma \varepsilon (T_s^4 - T_a^4) - \eta_c (T_s - T_a) \qquad \ldots\ldots (7)$$

The largest uncertainty in using equation (7) lies in the value adopted for the absorption coefficient of the painted surface, α. Measurements in the laboratory estimated it as 0.8. If $\frac{dT_s}{dt}$ and T_s are taken from the temperature profiles near the beginning of the fire then the re-radiation term in equation (7) is small and the precise value adopted for ε is unimportant; 0.95 was used. From the profiles in Figure 9 the incident fluxes were calculated as 58 kW/m², 25 kW/m² and 5.7 kW/m² for the LNG, LPG and kerosine fires respectively. For the LNG and LPG fires, for which the flame shape had been measured, the average surface emissive power was then estimated by calculating the view factors. The values calculated from the plates ranged from 131-169 kW/m² for the LNG fire, and 53-75 kW/m² for the LPG fire. These values compare well, on the whole, with those obtained from the wide-angle radiometers.

DISCUSSION

Flame Shape

A tilted cylinder has been used to represent the flame, and its elliptical base has enabled the downwind flame spill-over to be modelled. The reasonably low standard deviations of the mean surface emissive powers calculated from the various locations around the fires further supports the use of the model. Its major disadvantage is that it cannot fit the upwind flame edge which actually remains coincident with the edge of the bund. However, in the present tests only 2 of 21 radiometers were located upwind, and even their results were within the standard deviation produced by the other radiometers.

The measured burning rates appear, when compared with previous data for LNG (1) and kerosine fires (2), to be at their maxima. Therefore, Thomas' correlation, equation (1), reduces to $L/D \propto D^{-0.3}$. Previous comparisons with equation (1) have usually been made at small pool diameters where the mass burning rate has not yet reached its maximum. The present flame lengths are about 10% greater than predicted by the correlation for LNG and LPG, which may be adequate for most hazard analyses. However, although it remains the best correlation at present available it is not certain that it will be valid for still larger fires.

Surface Emissive Powers

The AGA land-based pool fires (1) were analysed independently by two teams. Welker (see ref. 1) predicted a limiting surface flux for large fires of 142 kW/m² by extrapolating the narrow-angle radiometer results without correcting for atmospheric transmission losses. If the correction had been

made, then Welker's limiting value would have been 180 kW/m^2 which is closer to the values measured by the narrow-angle radiometers during the present test. Atallah and Raj (see ref. 1), on the other hand, suggested a maximum value of 100 kW/m^2, despite the fact that the last readings obtained during the 24 m fire were close to 100 kW/m^2 and still rising. More recently, LNG pool fires have been performed on water at China Lake with pool diameters upto 15 m (5). The mean surface emissive powers calculated from both wide and narrow-angle radiometer measurements were about 220 kW/m^2, although the scatter in the data was large, especially from the wide-angle instruments.

For the present LNG fire the average surface emissive power was 153 kW/m^2. The difference between this value and the narrow-angle radiometer results of greater than 200 kW/m^2 is a clear indication that the radiative flux is not uniform over the surface of the flame. Apart from having temperature variations throughout, the flame is actually a volumetric rather than a surface emitter and will, therefore, be less emissive near its edges where the path length through the flame is shorter. The use of the solid flame model with the assumption of a surface emitter is a convenient concept to aid calculation techniques. In practice, the view of the wide-angle radiometers encompasses the less emissive portions as well as the sootier regions near the top of the flame.

For still larger fires, any increase in the radiation from the most emissive parts will depend on the path length through the flame and whether it is continuous. For example, it is probable that in large flames a central core of unburnt fuel exists for some way up the plume; this might then limit the radiative path length within the flame. However, the average surface emissive power will always be less than the value obtained from the most emissive portion. Its value will also be affected by the quantity of black soot which is produced, and this depends on the size of the fire and the proportion of heavier hydrocarbons in the LNG.

For LPG the average surface emissive power from the present fire was 48 kW/m^2, only one third of that from the LNG fire. This low average value was entirely attributable to the soot masking of the luminous flame. A larger value of about 80 kW/m^2 was previously obtained from a 1.8 m diameter LPG fire (unpublished). This suggests that the maximum average surface flux for LPG fires occurs close to the pool diameter at which black soot formation starts to be significant. Further increases in pool diameter will then produce more soot and hence lower average surface fluxes. This is demonstrated more clearly for kerosine. Hägglund and Persson (2) found that for kerosine fires a maximum surface flux of 130 kW/m^2 occurred at a pool size of 2 m, while at 10 m the soot reduced this to only 60 kW/m^2. The present 20 m fire has reduced this still further to about 35 kW/m^2.

CONCLUSIONS

The results from the tests described above should allow a more accurate assessment of the thermal radiation from large pool fires. In particular the radiation from large LPG fires can now be assessed independently without the need to refer to LNG data. The main conclusions are:

1. The flame shape for large pool fires may be represented by a tilted cylinder.

2. The flame tilt angle may be predicted using either equation (2) or (3).

3. Thomas' correlation appears to be adequate for predicting the flame length for pool fires upto at least 20 m in diameter.

4. The average surface flux for the LNG fire was 153 kW/m^2. The narrow-angle radiometers gave values up to 219 kW/m^2.

5. For the LPG fire the average surface flux was 48 kW/m^2. For larger fires an even lower value might be appropriate.

6. For the kerosine fire the narrow-angle radiometers measured a surface flux of about 35 kW/m^2.

7. The mass burning rates were determined to be 0.106 kg/m^2 s for LNG, 0.13 kg/m^2 s for LPG and 0.06 kg/m^2 s for kerosine.

SYMBOLS USED

A = area (m^2)

c = specific heat of metal plate (kJ/kg K)

D = pool diameter (m)

d = thickness of metal plate (m)

E = average surface emissive power (kW/m^2)

F = view factor

g = acceleration due to gravity (m/s^2)

L = flame length (m)

$\dot{m}$ = mass burning rate (kg/m^2 s)

q = thermal radiation flux (kW/m^2)

R = distance between flame element and receiving surface (m)

T = temperature (°C)

t = time (s)

U_w = wind speed (m/s)

α = absorption coefficient of painted metal surface

ε = emissivity of painted metal surface

η = convective heat transfer coefficient (kW/m^2 K)

θ = tilt angle from vertical (deg.)

ν = kinematic viscosity (m^2/s)

ρ = density (kg/m^3)

σ = Stefan-Boltzmann constant (kW/m^2K^4)

τ = atmospheric transmission coefficient

Subscripts

a = air

s = surface

v = vapour

REFERENCES

1. American Gas Association, 1974, "LNG Safety Program - Interim Report on Phase II Work", Report No. IS-3.1.

2. Hägglund, B. and Persson, L., 1976, "The Heat Radiation From Petroleum Fires", Försvarets Forskningsanstalt, Stockholm, FOA Report C20126-D6.

3. Thomas, P.H., 1963, "The Size of Flames From Natural Fires", 9th Symposium (International) on Combustion, Academic Press, New York.

4. Welker, J.R. and Sliepcevich, C.M., 1966, Fire Technology, 2, 127.

5. Raj, P.P.K., 1977, "Calculation of Thermal Radiation Hazards From LNG Fires - A Review of the State-of-the-Art", AGA Transmission Conference, St. Louis, Missouri, U.S.A.

6. Raj, P.P.K., Moussa, A.N. and Aravamudan, K., 1979, "Experiments Involving Pool and Vapour Fires From Spills of LNG on Water", Prepared for U.S. Coast Guard by A.D. Little Inc., Report No. C6-D-55-79.

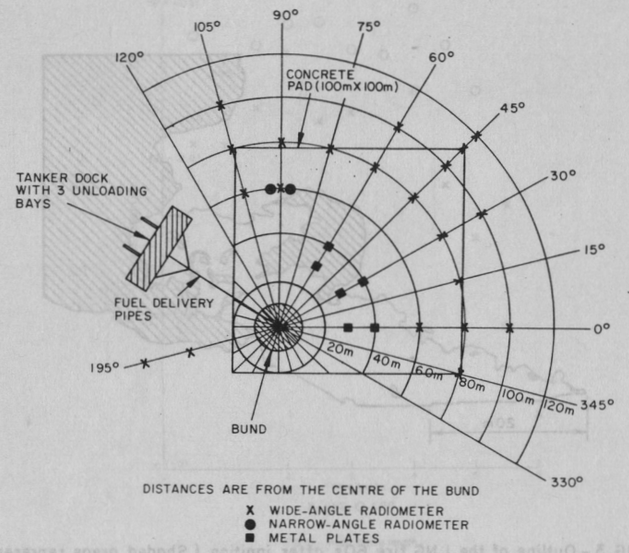

FIG. 1 - Layout of test facility and radiometers

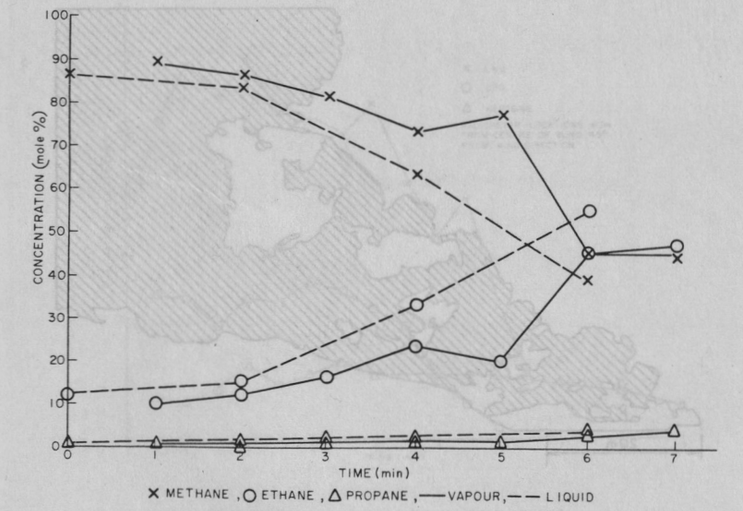

FIG. 2 - LNG composition during the fire

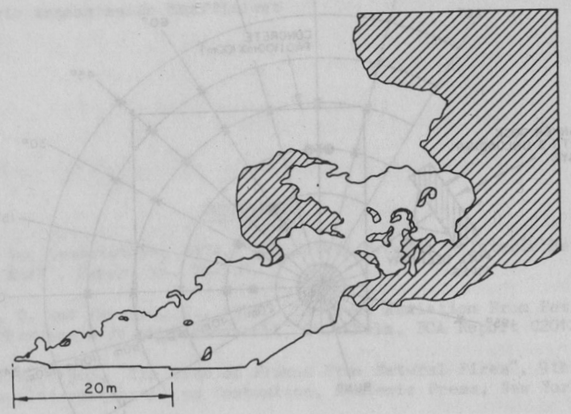

FIG.3 - Outline of the LNG fire 60s after ignition (Shaded areas represent black soot)

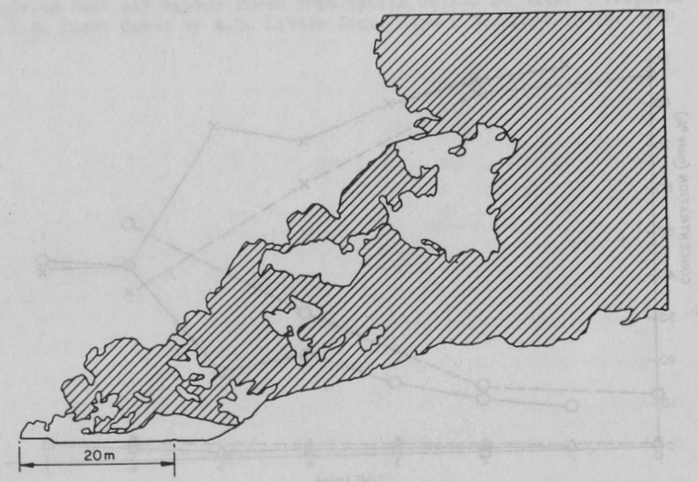

FIG.4 - Outline of the LPG fire 70s after ignition (Shaded areas represent black soot)

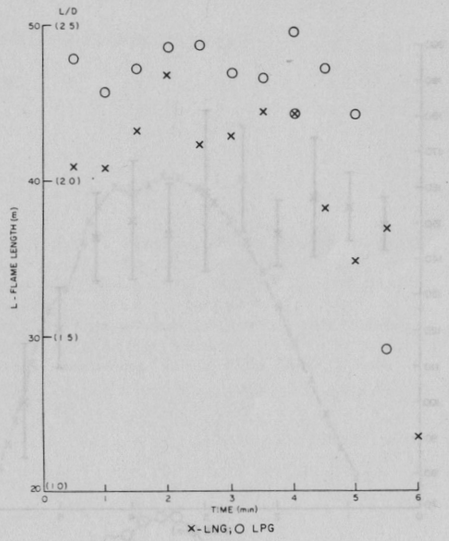

FIG.5 - Mean flame length

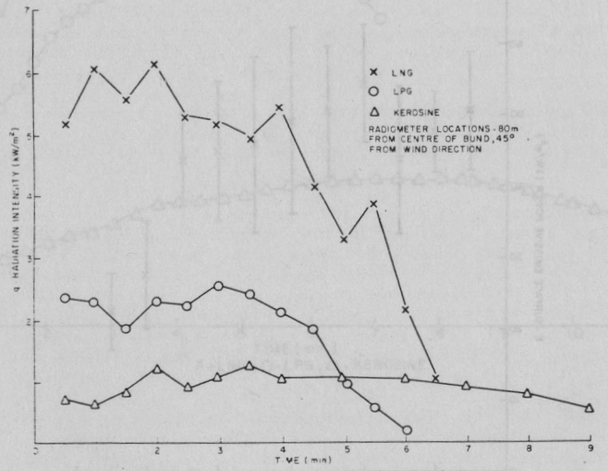

FIG 6 - Comparison of the radiation intensity from the LNG, LPG, Kerosine fires

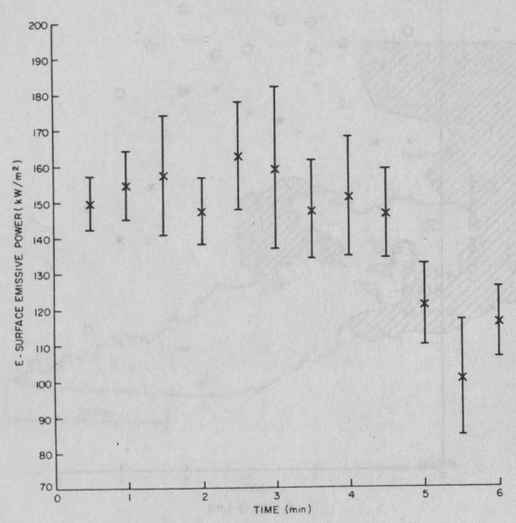

FIG. 7 - Surface emissive powers from the LNG fire

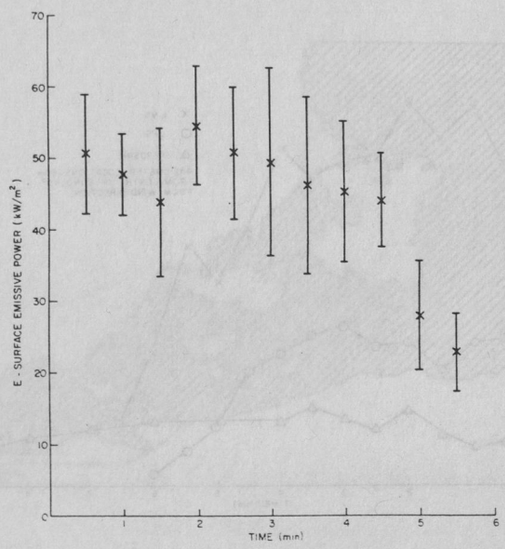

FIG 8 - Surface emissive powers from the LPG fire

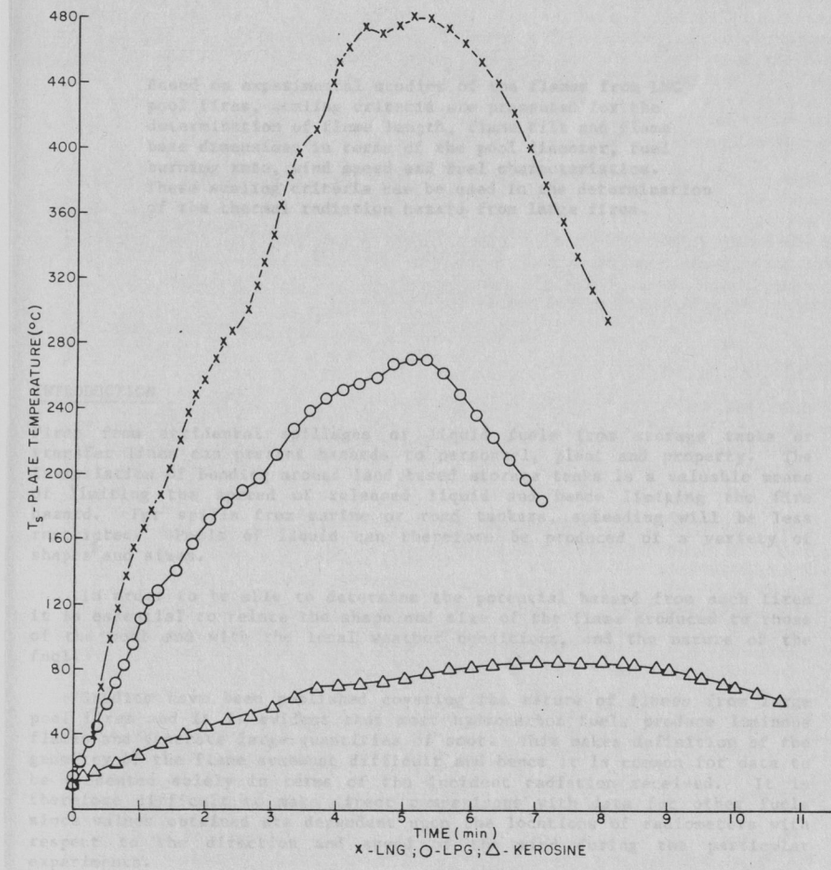

FIG. 9 - Plate temperatures during the LNG, LPG and kerosine fires